Research Square

Preprints are preliminary reports that have not undergone peer review.
They should not be considered conclusive, used to inform clinical practice,
or referenced by the media as validated information.

Water Pre-Positioning for Wildfire Suppression in Peru: Reservoir Coverage, Contingent Allocation, and ENSO-Modulated Adequacy (2001-2024)

Joel Cruz Machacuay

joelcruzmachacuay123@gmail.com

Universidad Privada del Norte Facultad de Ingenieria https://orcid.org/0009-0003-9974-1529

Juan Carlos Breña Aliaga

National Water Authority: Autoridad Nacional del Agua

Crhysley Sunny Berrios Romero

Peruvian Andes University: Universidad Peruana Los Andes

Research Article

Keywords: wildfires, ENSO, disaster risk reduction, remote sensing, Google Earth Engine, Peru

Posted Date: November 27th, 2026

DOI: https://doi.org/10.21203/rs.3.rs-11053533/v1

License: This work is licensed under a Creative Commons Attribution 4.0 International License.
Read Full License

Water Pre-Positioning for Wildfire Suppression in Peru: Reservoir Coverage, Contingent Allocation, and ENSO-Modulated Adequacy (2001-2024)

Joel Cruz Machacuay[1],*, Juan Carlos Breña Aliaga[2], Crhysley Sunny Berrios Romero[3]

[1] Universidad Privada del Norte, Av. Alfredo Mendiola 6062, Los Olivos, Lima 15306, Peru. ORCID: https://orcid.org/0009-0003-9974-1529

[2] Autoridad Nacional del Agua, Calle Diecisiete 355, Urb. El Palomar, San Isidro, Lima 15036, Peru. ORCID: https://orcid.org/0009-0004-2349-8654

[3] Universidad Peruana Los Andes, Av. Giraldez 231, Huancayo, Junín, Peru. ORCID: https://orcid.org/0009-0002-2492-1034

*Corresponding author: Joel Cruz Machacuay. Tel.: +51 997864499. E-mail: joelcruzmachacuay123@gmail.com

Abstract

Wildfire response in Peru relies on water sources with no formal geospatial planning, despite a reservoir and lake network of unknown adequacy. We develop a reproducible geospatial framework (Google Earth Engine, Python) integrating 2001-2024 fire recurrence stratified by El Niño-Southern Oscillation (ENSO) phase, a water inventory with allocable volume under contingent thresholds, source-to-fire accessibility, a Water Security Index for Suppression, and an optimization of new loading-point locations. Burned area is concentrated in the dry season (75% between August and October) and shows a one-year-lagged ENSO signal: national burned area correlates negatively with the contemporaneous Índice Costero El Niño (rho = -0.36) and positively with the prior year's Oceanic Niño Index (rho = +0.50; n = 24). This correlation does not survive correction for multiple comparisons, but the same lagged relationship replicates across three satellite products and a predictive model validated by temporal cross-validation. Peru's National Water Authority inventory (709 reservoirs, ~5,816 hm3 of usable storage; 13,522 operable lakes ≥ 2 ha) shows that water volume is not the limiting factor: 94% of reservoirs have recurrent fire within 20 km. The binding constraint is delivery: 22% of recurrent fire load lacks an adequate source within 15 km, and twenty optimally sited loading points would raise national coverage from 78% to 96%. Burned area nearly doubles (factor 1.93) in dry seasons following El Niño years, with the largest amplification in specific departments of the northern highlands and upper Amazon. The framework is open, reproducible, and transferable to other tropical Andean countries.

Keywords

wildfires; ENSO; disaster risk reduction; remote sensing; Google Earth Engine; Peru

Highlights

- A reproducible geospatial framework links wildfire recurrence, water inventory, and ENSO phase across Peru (2001-2024)
- National burned area shows a one-year lag with ENSO, replicated across three independent satellite fire products
- Peru's 709 reservoirs and 13,522 operable lakes show that water volume is not the limiting factor for suppression
- 22% of recurrent fire load lacks a water source within 15 km; twenty new loading points raise coverage from 78% to 96%
- Burned area nearly doubles in dry seasons following El Niño years, concentrated in specific high-priority departments

1. Introduction

The fire regime of the tropical Andes and the Amazon fringe of Peru is dominated by anthropogenic ignitions (approximately 98%; SERFOR 2024) over high-Andean herbaceous and shrub vegetation, puna grasslands, interandean dry forests, and humid transition forests. The critical window is the austral dry season (July-October). The 2016, 2023, and 2024 seasons registered extreme conditions, with tens of thousands of hectares affected, loss of life, infrastructure damage, and states of emergency declared in more than twenty regions (Defensoría del Pueblo 2024). Fire activity in the country also shows strong interannual modulation associated with the El Niño-Southern Oscillation (ENSO) cycle. Unlike most of the world, where operational monitoring relies on central Pacific indices (Niño 3.4 / ONI), the hydroclimatic variability of Peru's western slope responds more directly to sea surface temperature off the northern coast (Niño 1+2 region), synthesized in the Índice Costero El Niño (ICEN) of the ENFEN Multisectoral Commission. ICEN and ONI diverge frequently (e.g., the 2017 and 2023 coastal El Niño events), which motivates their joint use in this study.

Wildfire response in Peru faces a logistical water constraint that this interannual variability makes more consequential: aerial attack relies on bucket-equipped helicopters and sporadic international support, with no operational inventory of suitable water sources (reservoirs, lakes, qochas) and no criteria for the temporal allocation of volume to suppression. Geography compounds the problem, since most of the country's large reservoirs sit on the arid coast, built for irrigation, while recurrent fire foci are located in the highlands, at distances and elevation gains that can exceed a bucket-equipped helicopter's operational envelope.

Three gaps in the literature follow from this mismatch. First, the national-scale coverage of recurrent-fire areas by the reservoir and water-body network has not been quantified, nor has the fraction of that potential demand that could be met under contingent allocation thresholds. Second, how that adequacy degrades in El Niño years, when higher fire probability coincides with lower storage, has not been assessed. Third, no reproducible, open framework (Google Earth Engine and Python) exists that integrates ENSO-stratified fire recurrence, allocable water inventory, operational accessibility, and location optimization.

This paper addresses these three gaps using Peru's own open geospatial and administrative records. We map 2001-2024 burned-area recurrence and its probability stratified by ICEN/ONI phase, inventory reservoirs and natural water bodies to estimate allocable volume under 10/20/30% contingent thresholds, model source-to-fire operational accessibility to build a Water Security Index for Suppression, and assess how that adequacy degrades in El Niño years in order to prioritize locations for new loading points. Beyond the analysis itself, the framework provides the basis for a decision-support prototype that, given an ignition, would return prioritized water sources, allocable volume, estimated time of arrival, and cycles per hour.

2. Study Area

Continental Peru (approx. 1,285,000 km2), with emphasis on the high-Andean belt and the eastern piedmont between ~1,500 and 4,500 m a.s.l., where fire recurrence is concentrated. We characterize the major hydraulic infrastructure

network monitored by ANA (e.g., Poechos, San Lorenzo, Tinajones, Gallito Ciego, Condoroma, El Fraile, Aguada Blanca, El Pañe, Los Ejidos, Cuchoquesera, among others) and natural water bodies (high-Andean lakes and qochas).

3. Data

Table 1 summarizes the data sources used in this study.

Table 1 Data sources used in this study

Variable	Source / product	Resolution / period	Access
Burned area	MODIS MCD64A1 v6.1	500 m, monthly, 2000-2024	GEE
Active fire detections	VIIRS VNP14IMGML / FIRMS	375 m, 2012-2024	GEE / FIRMS
Fire validation	FireCCI51	250 m, 2001-2020	GEE
Water bodies	JRC Global Surface Water v1.4; Sentinel-2 MSI	30 m / 10 m, 1984-2021 / 2015-	GEE
Reservoirs and usable volume	ANA WFS geoservices: Publico/Presas (743), Publico/PrincipalesPresas (65)	vector, volume in hm3	geosnirh.ana.gob.pe
Minor reservoirs	ANA WFS: Publico/Reservorios (1,373, with Capacidad)	vector	geosnirh.ana.gob.pe
Natural lakes	ANA WFS: Publico/Lagunas (28,299 polygons)	vector	geosnirh.ana.gob.pe
Operational volume (time series)	Observatorio Nacional del Agua, reservoir volume	time series	snirh.ana.gob.pe
Water level (satellite)	ICESat-2 ATL13; Sentinel-3; SWOT	2018- / 2016- / 2023-	NSIDC / Hydroweb
Elevation	Copernicus GLO-30 DEM	30 m	GEE
Land cover / fuel	MapBiomas Peru; ESA WorldCover; MINAM ecosystems	10-30 m	GEE / MINAM
Precipitation / climate	CHIRPS; PISCO; ERA5-Land	0.05 / 0.1 degrees, daily	GEE / SENAMHI
ENSO	ICEN (ENFEN/IGP); ONI (NOAA CPC); E/C (Takahashi)	monthly, 1950-	IGP / NOAA
Population / assets	WorldPop; OSM (roads, heliports)	100 m / vector	GEE / OSM
Water quality (context)	ANA participatory monitoring (basins)	2012-2025 campaigns	ANA

4. Methods

4.1 ENSO indices and phase definition

ICEN is reconstructed as a three-month moving average of the sea-surface temperature anomaly in the Niño 1+2 region (ERSSTv5, 1981-2010 IGP climatology), and ONI is taken from NOAA CPC. For each year, the mean fire-season (Jul-Oct, JASO) ICEN and ONI are computed and the phase (El Niño, Neutral, La Niña) is classified according to the operational thresholds of ENFEN (2012) and NOAA. Years of divergence (a coastal-only or canonical-only event, sensu Takahashi et al. 2011) are identified for the sensitivity analysis.

4.2 Fire recurrence and stratified probability

For each year 2001-2024, a binary burn layer is generated from the MODIS MCD64A1 product (BurnDate > 0; Giglio et al. 2018) and summed to obtain recurrence (number of fire years per 500 m pixel), processed in Google Earth Engine (Gorelick et al. 2017); annual national and departmental (FAO GAUL) burned area and the monthly climatology are computed from the same layer. A gradient-boosted probabilistic fire model conditioned on ENSO is also fitted at the province-year level to isolate the ENSO effect from covariates of topography, fuel, seasonal climate, and fire memory; the full predictor set, algorithm, and validation strategy are given in Section 5.7. Recurrent fire foci are defined as cells with recurrence at or above a threshold (e.g., 3 of 24 years), and spatial clusters are delineated with DBSCAN.

4.3 Water inventory and allocable volume

For ANA reservoirs with a volume record, usable volume is taken and allocable volume is computed at 10/20/30% (parametric), net of minimum operating level and a reserve for environmental flow and irrigation commitments, with the choice of threshold treated in a sensitivity analysis. Natural water bodies are delineated with JRC Global Surface Water (occurrence > 75%; Pekel et al. 2016) and Sentinel-2 (NDWI), subject to a minimum operable area; their volume is approximated from area-volume relationships and satellite bathymetry (ICESat-2 / Sentinel-3 / SWOT level, where available), and water bodies below a minimum area/volume for bucket-helicopter operation are excluded.

4.4 Operational accessibility

A cost-distance surface over the Copernicus DEM is computed between each source and recurrent-fire cells and converted into cycle time (outbound-load-discharge-return) using a typical helicopter cruise speed (e.g., Mi-17) with an elevation-gain penalty. An altitude-density ceiling restriction reduces bucket volume and performance with elevation, with exclusion above an operational threshold, and a repositioning leg from a hub (Lima or other Peruvian Air Force bases) is included for support aircraft. The resulting metrics are cycles per hour, effective deliverable flow rate (L/h), and service radius.

4.5 Suppression water demand

A parametric range is adopted from the literature (critical flow per meter of fireline following Byram/Thomas formulations; equivalent orders of 1-4 L/m2 for direct attack on surface fires following Hansen 2012; aerial discharge capacity of 0.5-6 m3 per cycle depending on platform, and aerial suppression effectiveness following Plucinski 2019). Demand per focus is expressed per hectare and per fire-day and propagated by Monte Carlo simulation.

4.6 Supply-demand adequacy and index

For each focus or district, expected demand multiplied by recurrence is weighed against allocable volume accessible within the operational envelope. The resulting Water Security Index for Suppression (WSIS) is a function of recurrence, demand, nearby allocable volume, and accessibility, normalized to 0-1 and mapped by district. An El Niño stress test recalculates the index using El Niño-year fire probability together with the reservoir volume observed in El Niño years (low percentile), producing a gap map.

4.7 Location optimization

A maximal covering location model (MCLP, following the aerial-firefighting resource-siting formulation of Zeferino 2020) and a p-median model are used to propose locations for new loading points or helibases that maximize coverage of recurrent fire foci, weighted by recurrence and exposed population, subject to a budget constraint.

4.8 Reproducibility

The analysis is implemented as a repository of GEE-Python notebooks (geemap), with a pinned conda environment (environment.yml) and scripts to download indices from official sources and MINAM/ANA layers via OGC services. The code and derived tables are published with a versioned DOI on Zenodo.

5. Results

5.1 Fire recurrence and seasonality

Between 2001 and 2024, annual burned area detected by MODIS MCD64A1 in Peru ranged from ~12,100 ha (2001) to ~302,000 ha (2024), with a mean of ~118,100 ha/year and an increasing trend over the last decade. The years with the largest extent were 2024 (302,006 ha), 2005 (283,585 ha), 2022 (267,675 ha), 2010 (225,314 ha), 2020 (194,182 ha), and 2016 (182,137 ha). Seasonality is pronounced: August, September, and October account for 28.0%, 35.5%, and 12.0% of burned area respectively (~75.5% in the ASO quarter), and July through November together account for 90.5%.

The distribution is strongly regional. The departments with the largest cumulative burned area for 2001-2024 are Ucayali (551,190 ha), Cusco (332,495 ha), San Martín (249,676 ha), Huánuco (223,944 ha), Puno (208,134 ha), Madre de Dios (193,259 ha), Junín (176,740 ha), Apurímac (118,985 ha), Cajamarca (107,408 ha), and Ayacucho (94,265 ha); that is, a mix of Amazonian deforestation fire and high-Andean agropastoral fire.

Table 2 Annual burned area and JASO-season ENSO phase (2015-2024 excerpt; the complete 2001-2024 series is provided in the Zenodo data deposit, see Data Availability)

Year	Burned area (ha)	ICEN JASO	ONI JASO	ICEN JASO phase
2015	77,973	2.03	1.87	El Niño
2016	182,137	0.26	-0.37	Neutral
2019	132,361	-0.75	0.35	La Niña
2020	194,182	-1.09	-0.62	La Niña
2022	267,675	-1.23	-0.81	La Niña
2023	106,784	2.59	1.37	El Niño
2024	302,006	-0.66	-0.07	La Niña

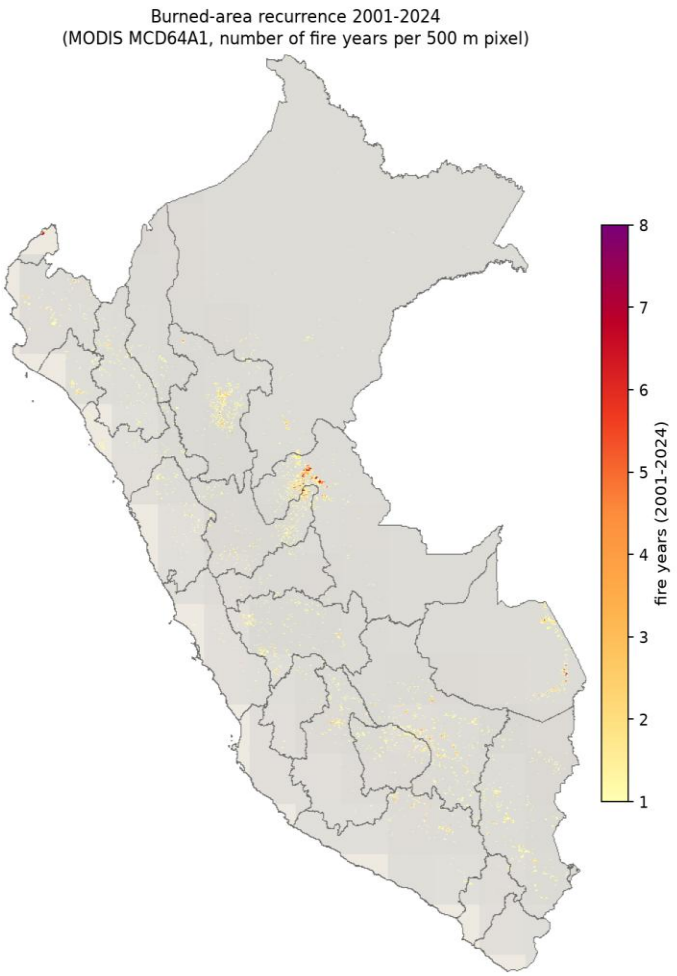


Fig. 1 *Burned-area recurrence 2001-2024 (MODIS MCD64A1): number of fire years per 500 m pixel. The signature is a diagonal Andean-piedmont band with cores in Huánuco-Ucayali and Cusco-Madre de Dios*

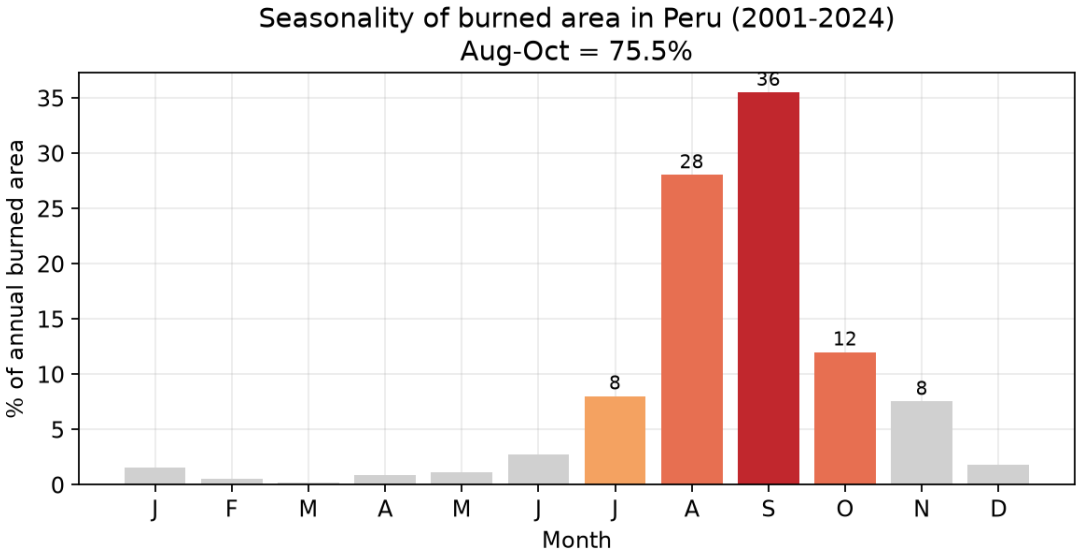


Fig. 2 *Seasonality of burned area: August-October accounts for 75.5%*

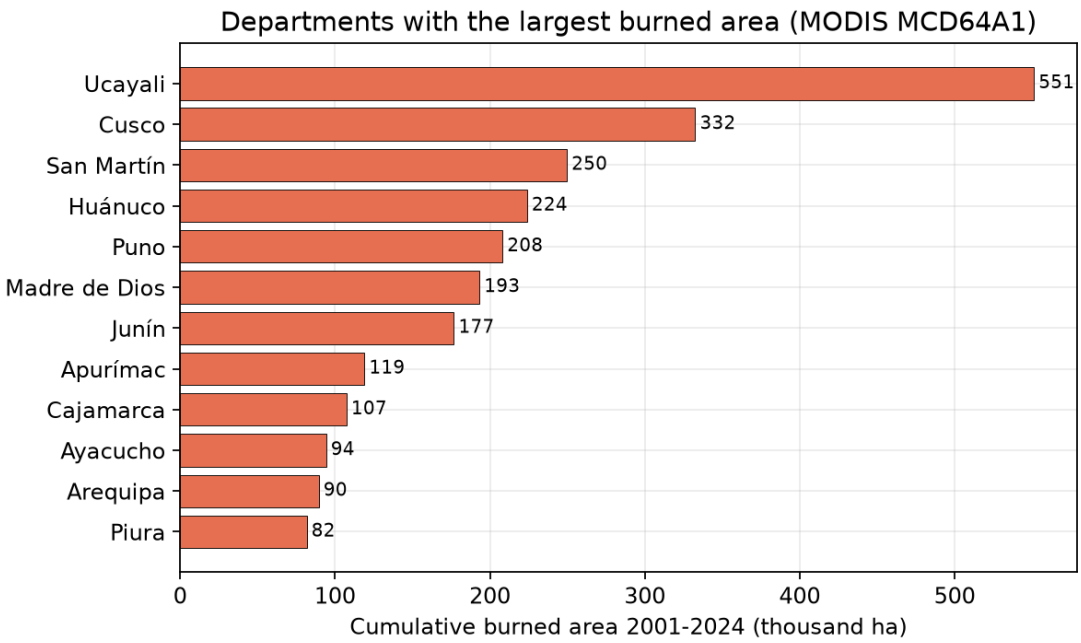


Fig. 3 *Departments with the largest cumulative burned area, 2001-2024*

5.2 ENSO Modulation

In contemporaneous terms, fire-season burned area is NOT higher in El Niño years: classifying by the mean July-October ICEN, the 6 El Niño years average ~76,500 ha (median 73,500), versus ~139,900 ha (median 114,800) in the 14 La Niña years and ~103,500 ha in the 4 neutral years; the pattern is analogous with ONI. The most extreme year in the series (2024) occurred under cold seasonal conditions, immediately after the strong 2023 El Niño (ICEN JASO 2023 = 2.59).

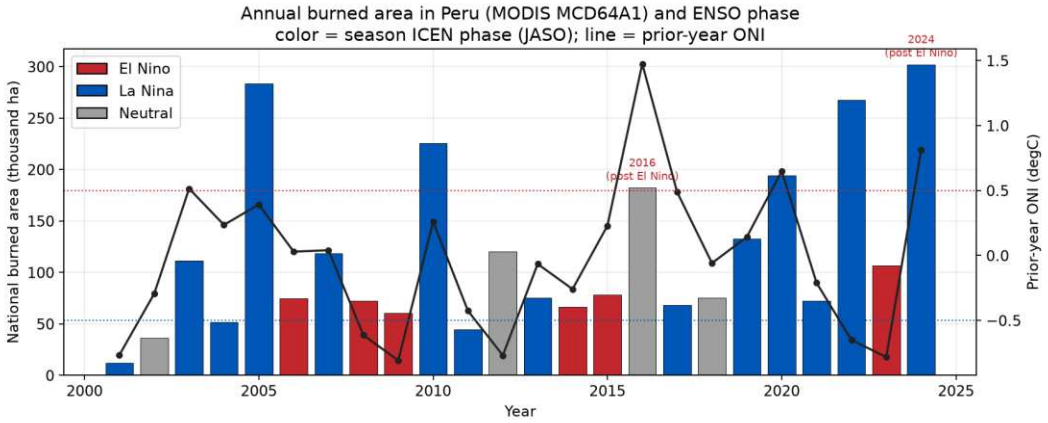


Fig. 4 *Annual burned area (bars, colored by JASO-season ICEN phase) and prior-year ONI (line). El Niño years (red) fall below the mean; the maxima (2005, 2022, 2024) are cold years following a high prior-year ONI*

5.2.1 Lag Structure

The Spearman correlation between annual national burned area and the ENSO indices suggests a lagged structure (n = 24, 2001-2024): with the contemporaneous season (JASO) ICEN the correlation is negative and marginal (rho = -

0.36; p = 0.084), whereas with the prior year's ONI it is positive (rho = +0.50; p = 0.014 uncorrected; 95% bootstrap CI [0.09, 0.80]). In the Andes, the prior year's ONI shows a similar pattern (rho = +0.42; p = 0.042 uncorrected). These two correlations are part of an exploratory sweep of 20 zone x predictor combinations (Section 5.8), and none survives correction for multiple comparisons (Benjamini-Hochberg, q = 0.05); they are reported here as exploratory, not confirmatory, evidence on their own. The strongest evidence for the lagged structure does not come from this exploratory table but from two independent sources: replication across three satellite products (Section 5.2.2, testing the same pre-specified ONI(t-1) hypothesis once per product) and the predictive model with spatial and temporal cross-validation (Sections 5.7 and 5.8), which shows a consistent, never-null improvement in predictive power from ENSO under independent partitions. With that caveat, the qualitative pattern is that the El Niño year itself tends to burn less, and it is the following year that records the largest fires (2016 after the 2015-16 El Niño; 2024 after the 2023-24 El Niño).

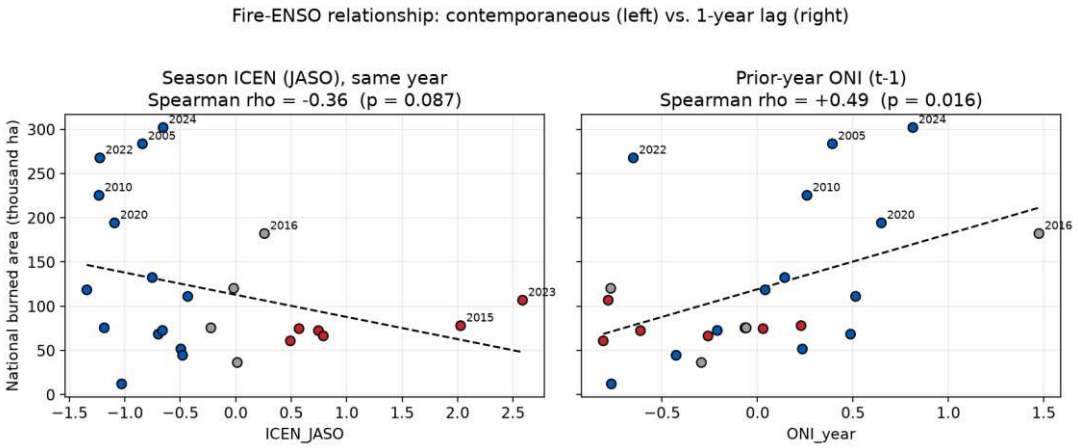


Fig. 5 *Fire versus ENSO: a negative contemporaneous relationship (left, ICEN JASO) versus a positive and significant lagged relationship (right, prior-year ONI)*

5.2.2 Multiproduct Robustness

The lagged structure is not an artifact of a single product. Recalculating the annual series with three independent satellite products, MODIS MCD64A1 (burned area, 500 m), ESA FireCCI51 (burned area, 250 m, 2001-2020), and MODIS MOD14A2 (active fire, 1 km), the Spearman correlation with the season ICEN is negative in all three (-0.27 to -0.36), and with the prior year's ONI it is positive, uncorrected-significant in all three (p = 0.016, 0.012, 0.049) and of similar or larger magnitude in all three (+0.41 to +0.55; FireCCI51 reaches +0.55). Unlike the sweep in Section 5.2.1, here a single pre-specified hypothesis (prior-year ONI) is tested in three independent samples, so replication of sign and order of magnitude is stronger evidence than an isolated p-value.

Table 3 Spearman correlation of fire with ENSO by independent satellite product (n=24, except FireCCI51 n=20 owing to its 2001-2020 temporal coverage)

Product	ICEN JASO (t)	ICEN (t-1)	ONI JASO (t)	ONI (t-1)
MCD64A1 (burned area)	-0.36	+0.30	-0.32	+0.49
FireCCI51 (burned area)	-0.33	+0.31	-0.41	+0.55
MOD14A2 (active fire)	-0.27	+0.25	-0.30	+0.41

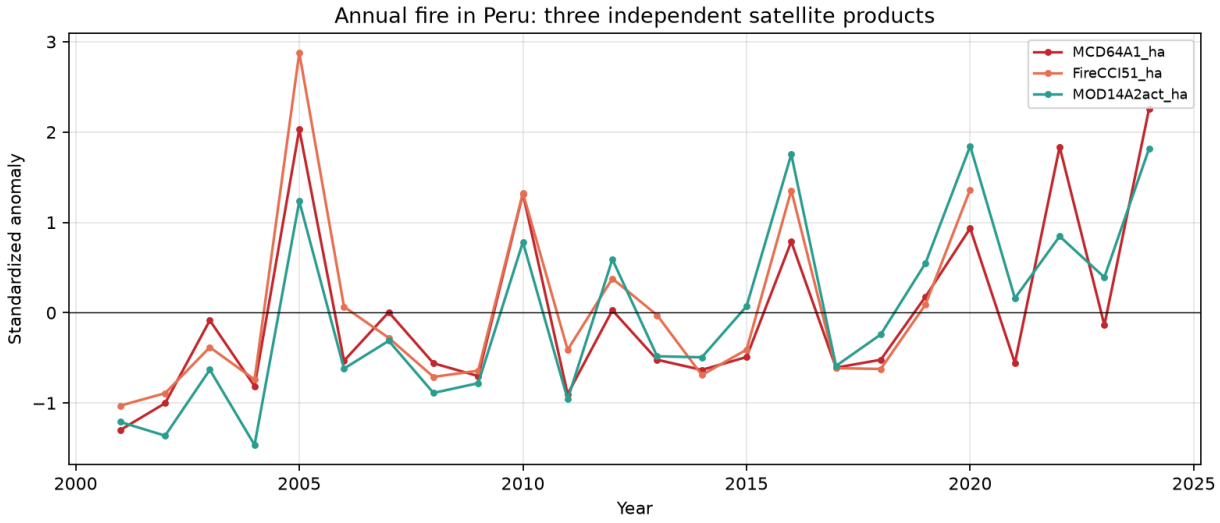


Fig. 6 *Annual fire anomaly in Peru (standardized) according to three independent satellite products; high co-movement (the 2005, 2016, and 2020 maxima coincide)*

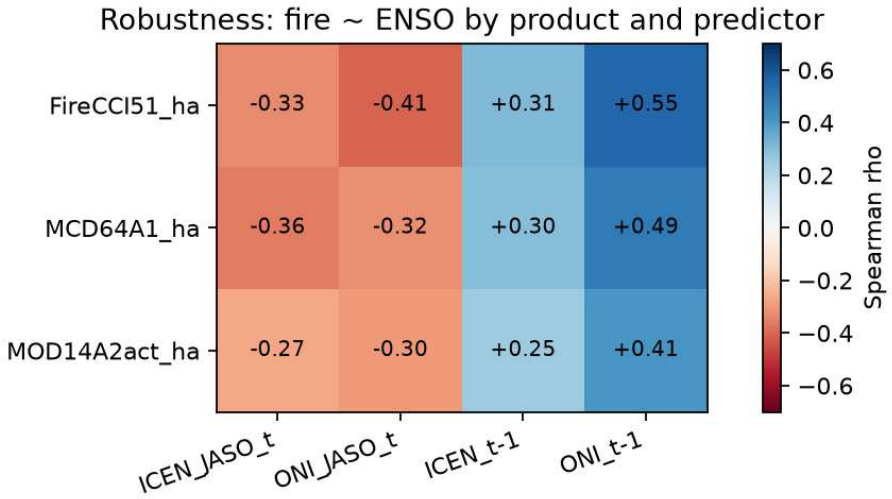


Fig. 7 *Fire-ENSO correlation by product and predictor: a negative contemporaneous relationship (left) and a positive lagged relationship (right) across all three products*

5.2.3 Macroregion Partition

The partition by elevation and longitude (Copernicus DEM) into Coast (<1000 m, west), Andes (>=1000 m), and Amazon (<1000 m, east) shows responses of differing sign. In the Amazon, FIRMS active-fire detections for 2001-2024 (1.37 million) dominate the national count, but burned area is lower in contemporaneous El Niño years (median 32,262 ha) than in La Niña years (56,568 ha), a significant difference with the season ONI (Mann-Whitney $p = 0.008$); the largest Amazonian years (2005, 2007, 2010, 2024) combine deforestation with lagged drought, consistent with ENSO-fire-land use interactions reported for the Brazilian Legal Amazon by Barbosa et al. (2021). The Andes concentrate the burned area of the extreme years (2005: 160,610 ha; 2016: 123,452 ha; 2020: 136,809 ha; 2022: 201,815 ha), with a contemporaneous response that is negative or null and a lagged response that is positive (prior-year ONI: El Niño ~77,500 ha vs. La Niña ~52,000 ha). The Coast shows a small burned area in absolute terms (0-

26,000 ha/year) but with maxima in coastal El Niño years (2017: 24,132 ha; 2023: 26,301 ha), consistent with an ephemeral fine-fuel pulse, the greening of the desert and coastal lomas by El Niño rainfall, that burns during the same dry season.

Table 4 Mean burned area by ENSO phase (contemporaneous and lagged) and Mann-Whitney U test, selected series

Series	Predictor	El Niño (ha, mean)	La Niña (ha, mean)	MWU p
National	ICEN JASO (t)	76,845	141,892	0.239
National	ICEN prior year (t-1)	158,523	104,151	0.245
National	ONI JASO (t)	69,700	156,047	0.138
Amazon	ONI JASO (t)	33,982	64,349	0.008
Andes	ONI prior year (t-1)	77,534	51,934	0.477
Coast	ICEN prior year (t-1)	12,825	6,711	0.202

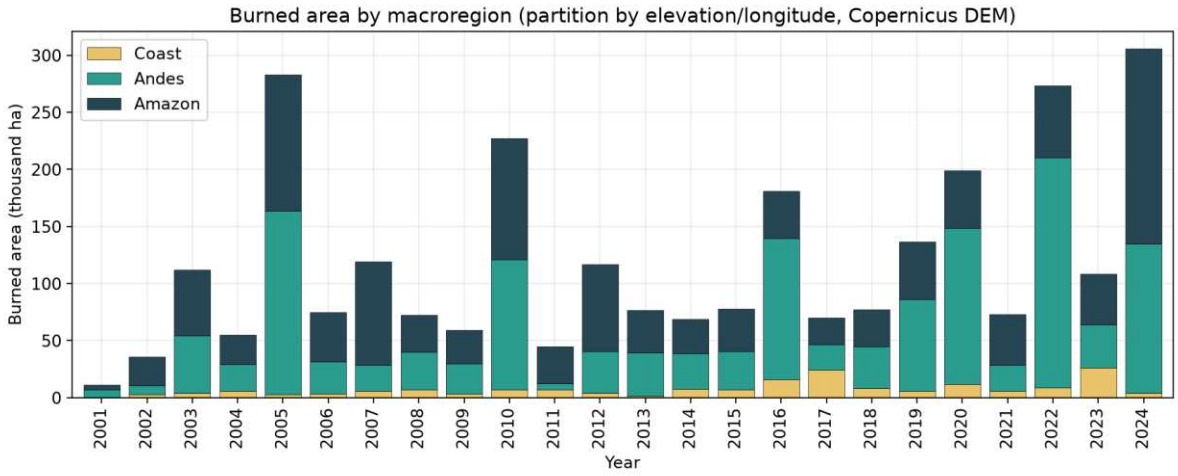


Fig. 8 *Annual burned area by macroregion. The Coast (yellow) reaches its maxima in 2017 and 2023, the two coastal El Niño years*



Fig. 9 *Macroregions used in the analysis (partition by elevation and longitude, Copernicus DEM)*

The annual sample size is small (n=24): effect sizes are reported, correction for multiple comparisons is applied (Section 5.8), and future work will extend the series with GFED (1997-) and VIIRS active-fire detections (2012-) at monthly resolution.

5.3 Water Inventory and Allocable Volume

From ANA's WFS geoservices (the public folder of geosnirh), 743 reservoirs were obtained (Presas layer); after removing duplicate dikes and repeated records, 709 remain, of which 278 report usable storage volume, totaling ~5,816 hm3. An additional 1,373 minor reservoirs are included (Reservorios layer; median 432 m3, total ~5.5 hm3, a negligible contribution) along with the 65-reservoir principal-dams layer. Contrary to the initial intuition, storage is not only coastal: the Andes and the piedmont concentrate ~4,376 hm3 of usable storage across 211 reservoirs (Lagunillas, 500 hm3, in Puno; Upamayo, 441 hm3, in Pasco; Aucceccocha, 375 hm3, and Choclococha, 131 hm3, in Huancavelica; Condoroma, 259 hm3, in Arequipa; Pomacanchi, 218 hm3, in Cusco), versus ~1,440 hm3 across 67 coastal reservoirs (Poechos, 396 hm3; Gallito Ciego, 367 hm3; Tinajones, 319 hm3; San Lorenzo, 196 hm3). The larger reservoirs in the ANA inventory match those recorded for Peru in the global GRanD dams and reservoirs catalogue (Lehner et al. 2011), used as a cross-check of names and locations.

Table 5 Allocable water volume under contingent thresholds, by macroregion (over the 278 reservoirs with reported usable volume)

Allocation threshold	Coast (hm3)	Andes/Amazon (hm3)	Total (hm3)
10% of usable volume	144	438	582
20% of usable volume	288	875	1,163
30% of usable volume	432	1,313	1,745



Fig. 10 *ANA reservoirs (n=709; point size proportional to usable volume) over fire recurrence. Reservoir density is high in the south-central Andes and coastal valleys, but the recurrent-fire core along the Huánuco-Ucayali border remains almost devoid of storage infrastructure*

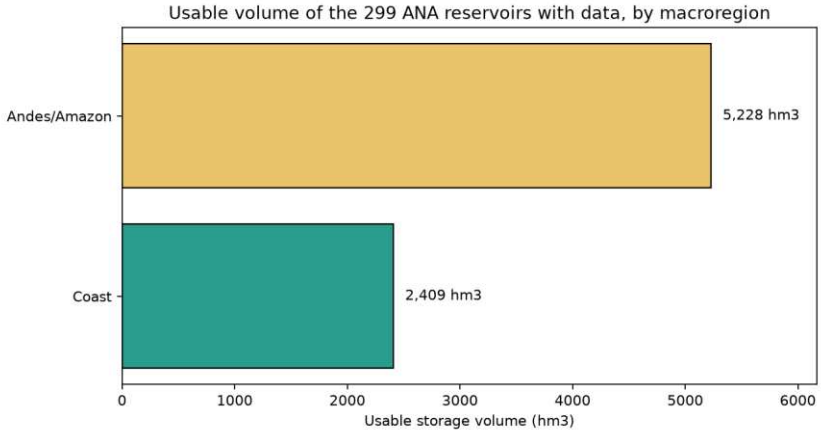


Fig. 11 *Usable storage volume by macroregion (278 reservoirs with data)*

Natural water bodies from the ANA Lagunas layer add to the reservoirs: of 28,242 polygons, 13,522 exceed 2 ha (the screening threshold for bucket-helicopter operation; depth is not recorded and is treated as an uncertainty) and 4,577 exceed 10 ha, with ~9,210 km2 of operable surface, concentrated in the Carabaya, Central, Blanca, La Viuda, Chonta, and Huaytapallana mountain ranges. The combined source inventory totals 14,231 points (709 reservoirs + 13,522 operable lakes).

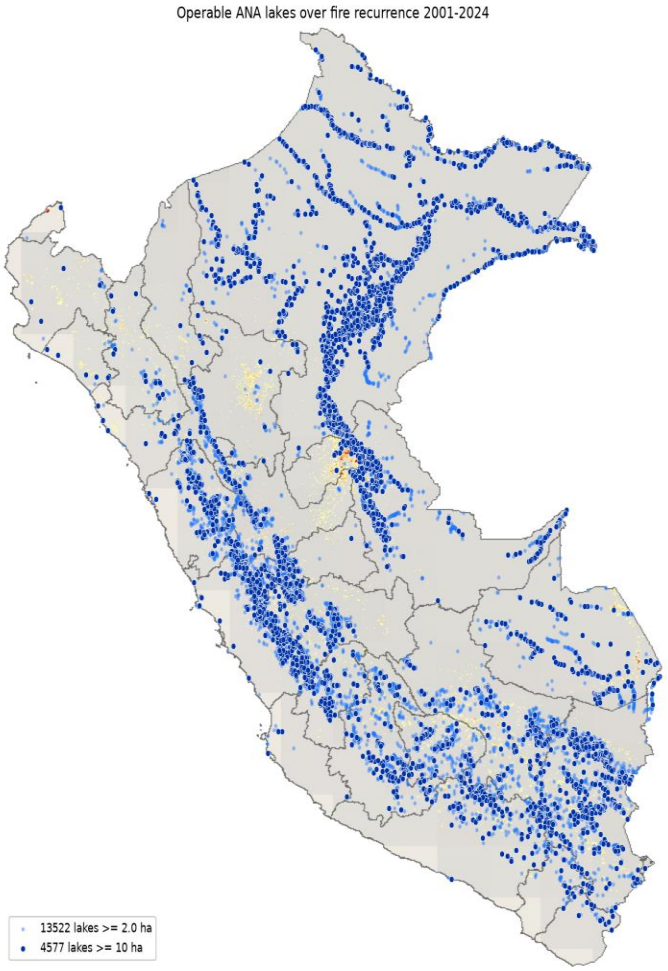


Fig. 12 *Operable ANA lakes (≥2 ha in light blue, ≥10 ha in dark blue) over fire recurrence. The high-Andean lake network spatially coincides with most of the Andean fire signal*

The spatial overlay (20 km buffer, MODIS recurrence) was run on the full WFS list of 743 reservoirs (prior to deduplicating dikes and repeated records to 709; deduplication does not affect the geographic position of real reservoirs, it only removes administrative duplicates, so the percentage is valid under either denominator): 699 of 743 (94%) have burned area within 20 km in 2001-2024, and 249 (34%) have recurrent fire (>=3 years) within that radius. For a typical 100-500 ha fire and a direct-attack rate of 1-4 L/m2, water demand is on the order of 0.002-0.01 hm3 per event, so that even the 10% allocable volume (582 hm3, computed over the 709 deduplicated reservoirs) covers tens of thousands of events. The binding constraint is not aggregate volume but delivery and the existence of a source within operational reach, quantified in Section 5.4.

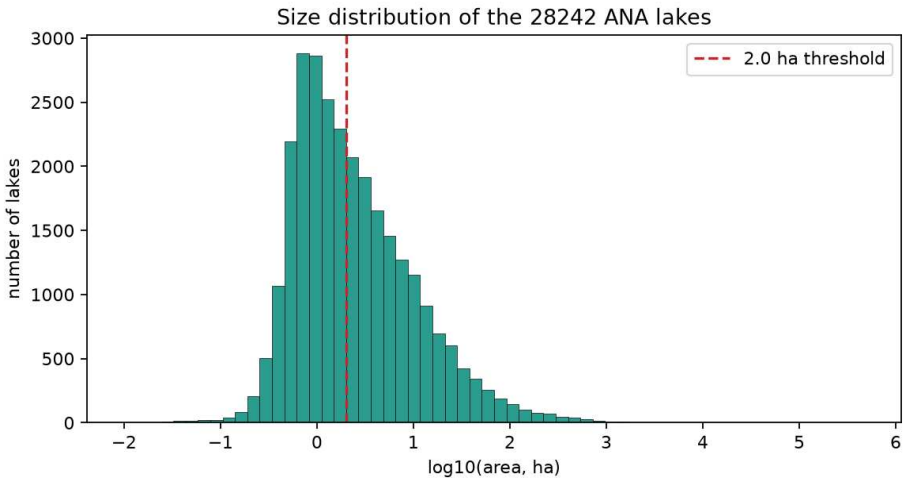


Fig. 13 *Size distribution of the 28,242 ANA lakes (log scale); ~48% exceed 2 ha*

5.4 Operational Accessibility and the Water Security Index for Suppression

On a 2 km grid, 1,004 cells with recurrent fire were identified (>=2 years in 2001-2024; weighted load = 2,738 cell-years). For each cell, the distance to the nearest water source in the combined inventory was computed (k-d tree in an azimuthal equidistant projection), along with helicopter cycle time (t = 3 fixed minutes for load-discharge-maneuvering plus a round trip at 180 km/h), cycles per hour, the deliverable flow rate with a 2,000 L bucket, and an altitude-density performance penalty (onset at 2,500 m, minimum factor 0.45).

The median distance to the nearest source is 8.9 km, with a 90th percentile of 22.1 km and a maximum of 72.9 km; the nearest source is a lake in 938 of 1,004 cells and a reservoir in 66. Coverage of fire load within 15 km, the reference operational radius, is 78%, rising to ~92% at 22 km and saturating toward 98% at 35 km (Fig. 14); that is, ~22% of recurrent fire lacks an adequate source within useful range. Cycles per hour have a median of 6.7, and the deliverable flow rate per helicopter has a median of ~11,800 L/h; the altitude penalty is marginal at the median (factor 1.00) because MODIS-detected recurrence is dominated by the lowland Amazon, and it is expected to matter more once high-Andean grassland fire is incorporated through VIIRS detections.

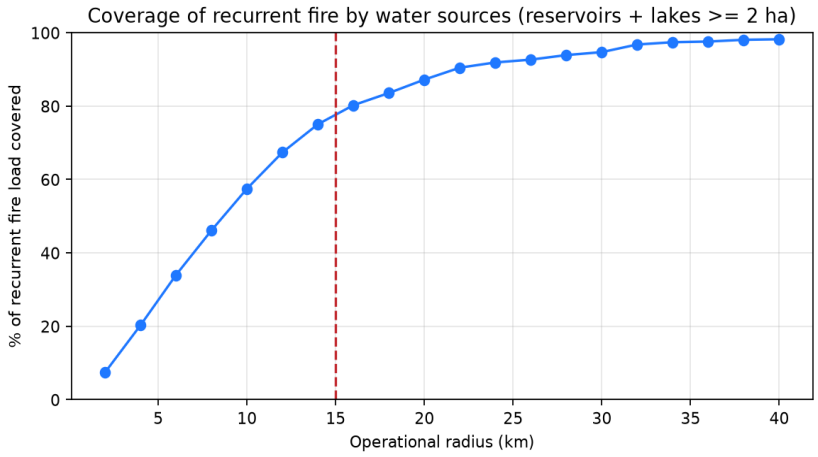


Fig. 14 *Coverage of recurrent fire load as a function of operational radius. At 15 km, 78% is covered*

Aggregating to the district level (GAUL level 2; 113 districts with recurrent fire), the Water Security Index for Suppression (WSIS, 0-1) was built as a combination of coverage at 15 km (0.45), proximity to source (0.35), and deliverable flow rate (0.20). The districts with the largest gap (WSIS close to 0) lie in the northern highlands and the upper Amazon fringe: Morropón and Ayabaca (Piura), Utcubamba and Luya (Amazonas), El Dorado, Tocache, Rioja, and Mariscal Cáceres (San Martín), Oxapampa (Pasco), Chota and Cutervo (Cajamarca), Pachitea (Huánuco), Satipo (Junín), and Tumbes. Among districts with the highest fire load, Coronel Portillo (Ucayali, 835 cell-years) is well covered (WSIS 0.78), but Puerto Inca (Huánuco), Bellavista, and Mariscal Cáceres (San Martín) combine high load with low coverage (WSIS 0.32, 0.21, and 0.14): these are the priority districts.

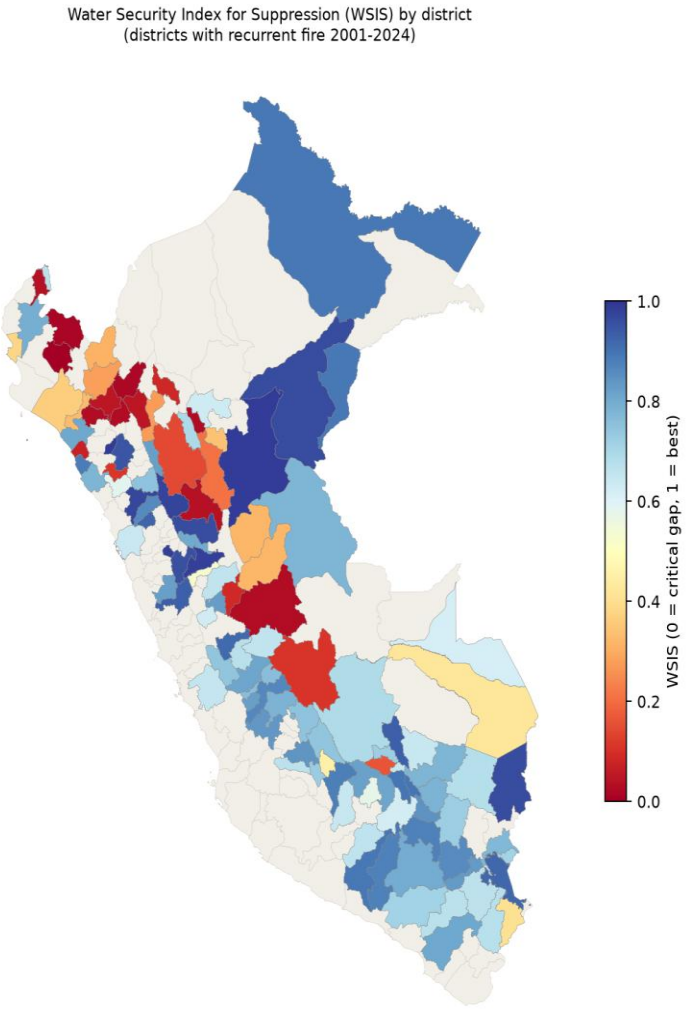


Fig. 15 *Water Security Index for Suppression (WSIS) by district. Red: critical gap (northern highlands and upper Amazon fringe); blue: adequate source within reach (lowland Amazon in Ucayali and Madre de Dios, south-central Andes)*

The district ranking is robust to the choice of WSIS weights (Spearman >= 0.76 against four alternative schemes, Section 5.8). Model limitations are discussed in Section 6.4 (Euclidean versus terrain-cost distance; MCD64A1 underdetects grassland fire; illustrative helicopter parameters).

5.5 Loading-Point Location Optimization

The 230 recurrent-fire cells without a source within 15 km (load 601 cell-years, 22% of the total) were taken as demand for a maximal covering location model (MCLP), solved with a greedy submodular algorithm. The scope of this exercise must be stated precisely: the loading-point candidates are the coordinates of the discovered fire cells themselves (not verified sites with road access, land tenure, or an actual water body), so the result is an idealized upper bound on what is achievable, useful for prioritizing search areas for real sites rather than for selecting final installation coordinates. With that caveat, marginal performance is high: 10 new loading points raise national coverage from 78% to 92.8%, 20 points to 95.8%, and 30 points to 97.1% (Fig. 16). The first 20 points are concentrated in the upper Amazon fringe of San Martín, Amazonas, and Huánuco, the edge of the Huánuco-Ucayali core, Madre de Dios, and the northern coast (Tumbes-Piura); most at 200-500 m elevation, except for one high-Andean point (~4,100 m) on the Apurímac-Cusco border.

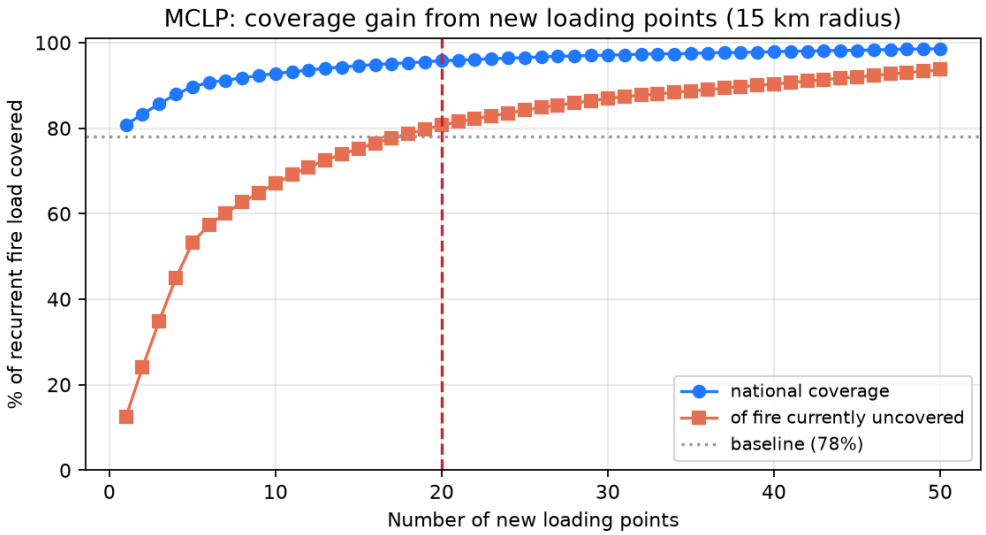


Fig. 16 *Coverage of recurrent fire load as a function of the number of new loading points (MCLP, 15 km radius). Twenty points raise coverage from 78% to 96%*

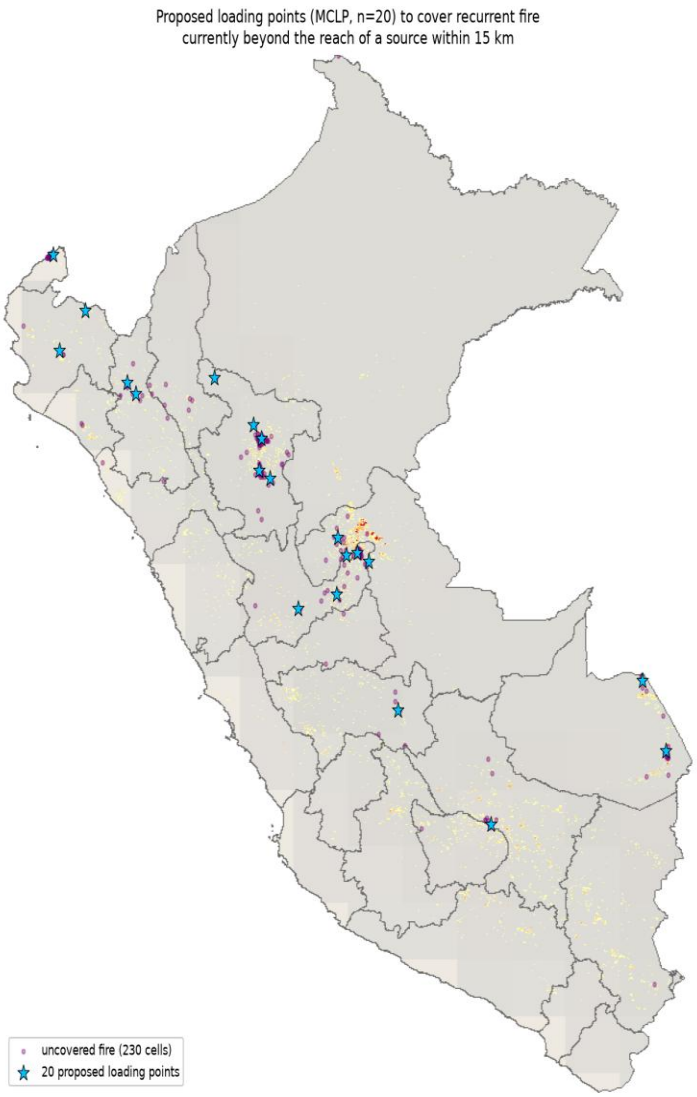


Fig. 17 *Twenty proposed loading points (stars) over the 230 recurrent-fire cells currently without an adequate source within 15 km (purple points)*

Future work (a priority before any operational proposal): restrict candidates to real water bodies or verifiable road infrastructure, and incorporate site-development cost, land tenure, and exposed population as weights.

5.6 Stress Test: Dry Seasons Following El Niño

Definitional note: this section uses a year-classification criterion different from the contemporaneous-season ENSO phase (JASO ICEN/ONI, used in Section 5.2 and Table 2). Here, 'post-El Niño' refers to the mean ONI of the PRIOR YEAR, so a year can be 'post-El Niño' under this criterion while simultaneously 'La Niña' under its own season's contemporaneous phase (this is exactly what happens in 2020 and 2024; see Table 2): both are compatible, and this is precisely the lag mechanism documented throughout the paper (El Niño in year N, amplified fire in year N+1, which can itself be physically cold).

Fire years 2001-2024 were classified by the prior year's mean ONI: post-El Niño (ONI(t-1) >= 0.5): 2003, 2016, 2020, and 2024. Nationally, the mean burned area of those seasons is ~197,350 ha versus ~102,140 ha in the remaining years (factor 1.93). Amplification is largest in La Libertad (x7), Cajamarca (x5), Huancavelica and Áncash (x4), and Madre de Dios, Amazonas, Junín, and Ayacucho (x3). Crossing that amplification with the department-aggregated WSIS yields a double-pressure index (more fire after El Niño plus lower water security): Cajamarca, Amazonas, Madre de Dios, La Libertad, Tumbes, Pasco, Junín, and San Martín rank highest. These are the territories where an ENFEN El Niño forecast should trigger pre-positioning 12-18 months in advance.

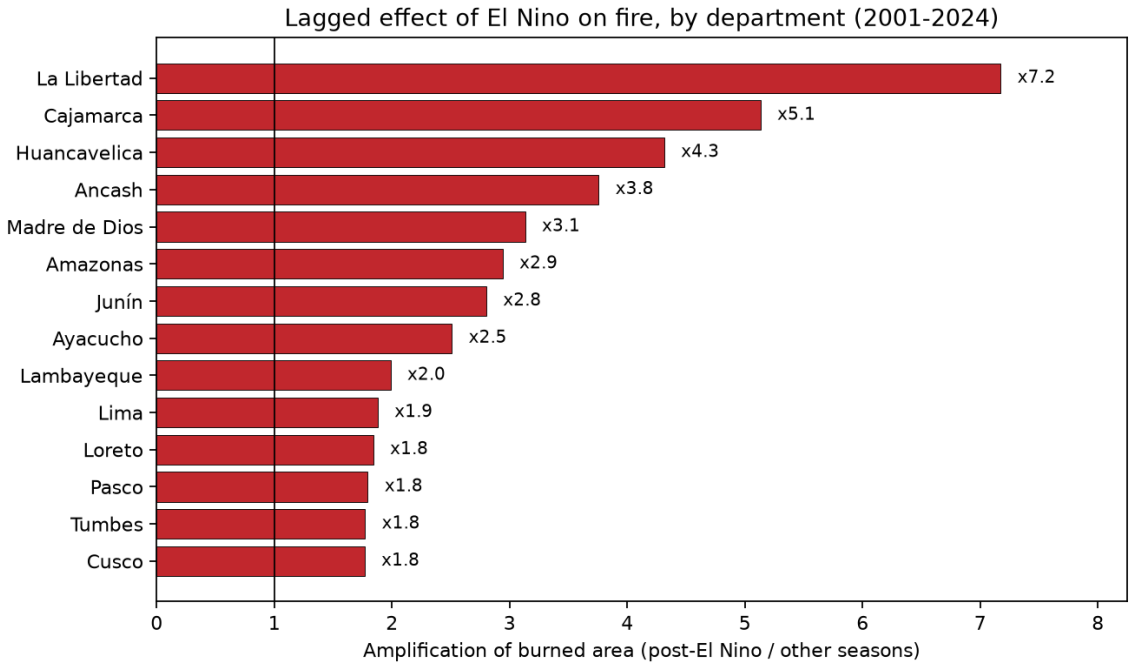


Fig. 18 *Amplification of burned area in post-El Niño seasons relative to other seasons, by department (2001-2024; departments with a baseline >= 200 ha/year)*

Future work: also stress-test reservoir volume (ANA Observatory time series) for the WSIS deliverable-flow term.

5.7 Probabilistic Fire Model Conditioned on ENSO

To separate the ENSO effect from its covariates, a gradient-boosted tree model (HistGradientBoosting) was fitted on a panel of 193 provinces x 24 years (n = 4,439 province-years; response variable: MODIS burned area > 0.2% of the province; base rate 17%). The base predictors are topography (elevation, slope), fuel (fractions of tree, grassland, cropland, and urban cover; maximum NDVI of the prior wet season and minimum NDVI of the dry season), seasonal climate (TerraClimate: wet- and dry-season precipitation, maximum temperature, vapor pressure deficit, soil moisture, PDSI), and fire memory (burned fraction in the prior year). Predictive power was evaluated with spatial block cross-validation (6 folds by department).

Under spatial cross-validation by department (6 folds), adding ENSO raises AUC from 0.72 (covariates only) to 0.77 and PR-AUC from 0.33 to 0.43; ICEN and ONI contribute essentially identical power (AUC 0.774 vs. 0.769), so for fire, unlike coastal hydrology, what matters is the lag of the ENSO cycle rather than which index is used. In

permutation importance, the two ENSO terms are the dominant predictors, with prior-year ICEN ranking first and season ICEN second, ahead of NDVI, cropland fraction, prior burned fraction, and PDSI, and the partial dependence shows fire probability increasing with prior-year ICEN (Fig. 21). In the post-El Niño scenario, with prior-year ICEN at its 90th percentile, modeled fire probability is amplified by a factor of 1.28 at the provincial median and 1.86 at the 90th percentile, with the highest values in the central jungle (Huánuco-Ucayali), the northern coast and highlands (Piura), and the southern highlands (Cusco-Apurímac-Puno) (Fig. 22).

Spatial CV by department shares the same year, and therefore the same ICEN/ONI value, between training and test, because ENSO is a national scalar per year. To isolate forecast skill for a never-seen ENSO year, the fit was repeated with strict temporal validation (leave-one-year-out, 24 folds, each holding out one full year): the AUC improvement from ENSO remains positive but drops to +0.014 (0.802 vs. 0.788), compared with +0.06 under spatial CV. This is the operationally relevant estimate, since it corresponds to the real case of forecasting a fire season before it occurs, and it confirms that ENSO carries genuine forecasting signal, albeit of more modest magnitude than suggested by spatial CV alone (Section 5.8).

Table 6 Predictive power (AUC, spatial cross-validation by department) of the fire model with ICEN, with ONI, and without ENSO

Model	**AUC (spatial CV)**	**PR-AUC**
Covariates + ICEN	0.774	0.430
Covariates + ONI	0.769	0.432
Covariates only (no ENSO)	0.715	0.324

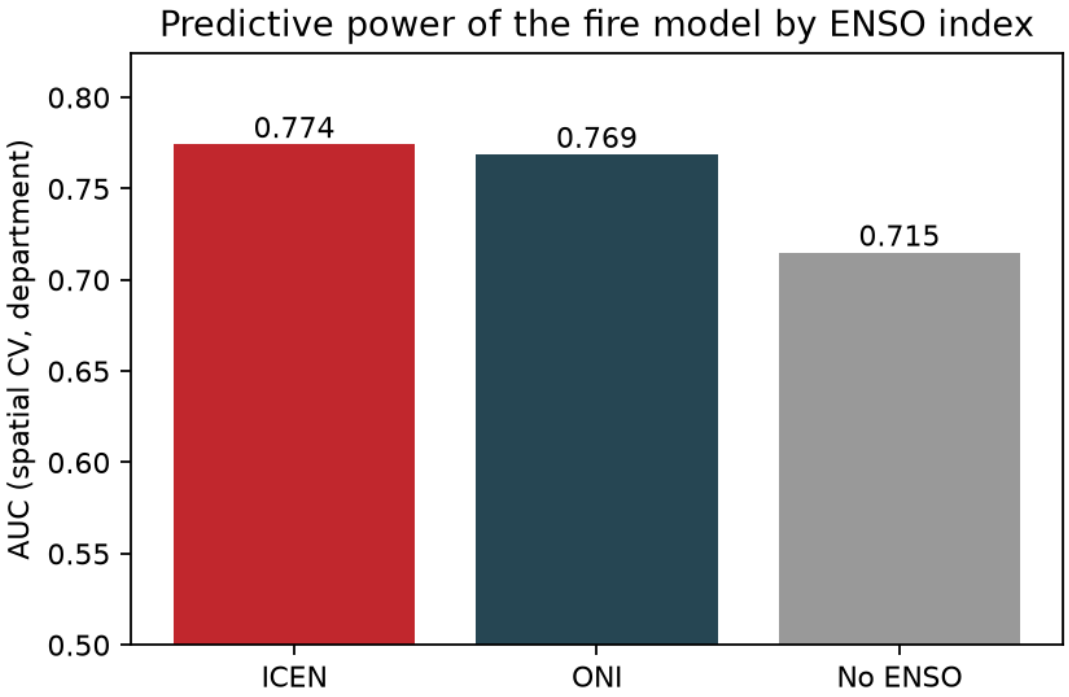


Fig. 19 *Predictive power (AUC, spatial cross-validation) of the fire model with ICEN, with ONI, and without ENSO*

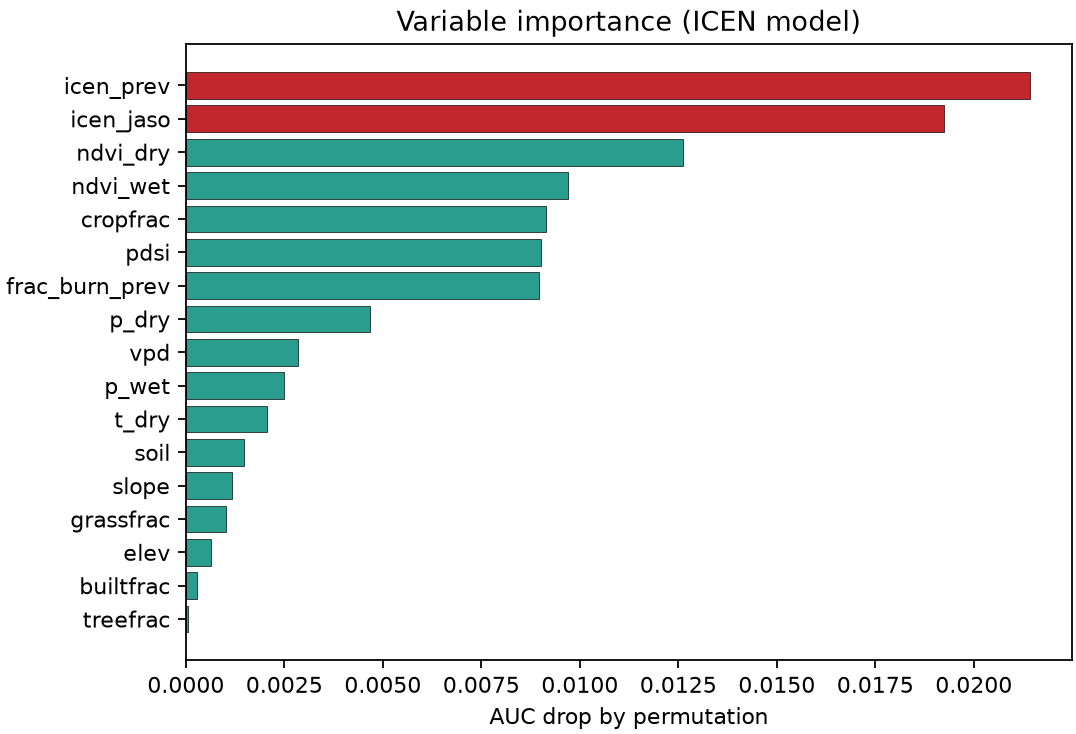


Fig. 20 *Permutation variable importance (AUC drop). ENSO terms are shown in red and top the ranking*

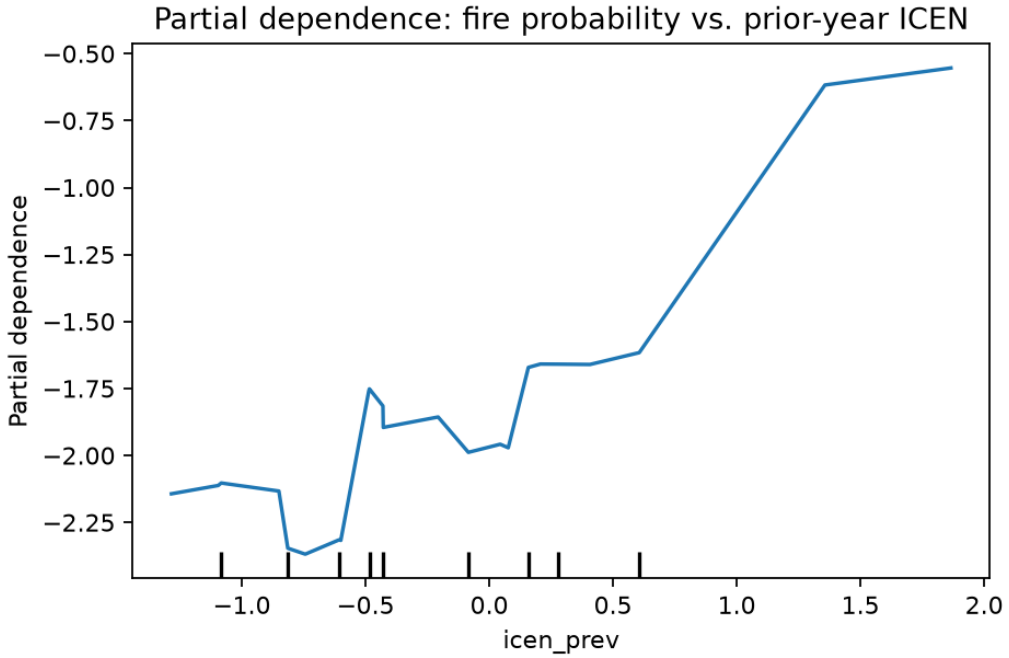


Fig. 21 *Partial dependence: fire probability as a function of prior-year ICEN*

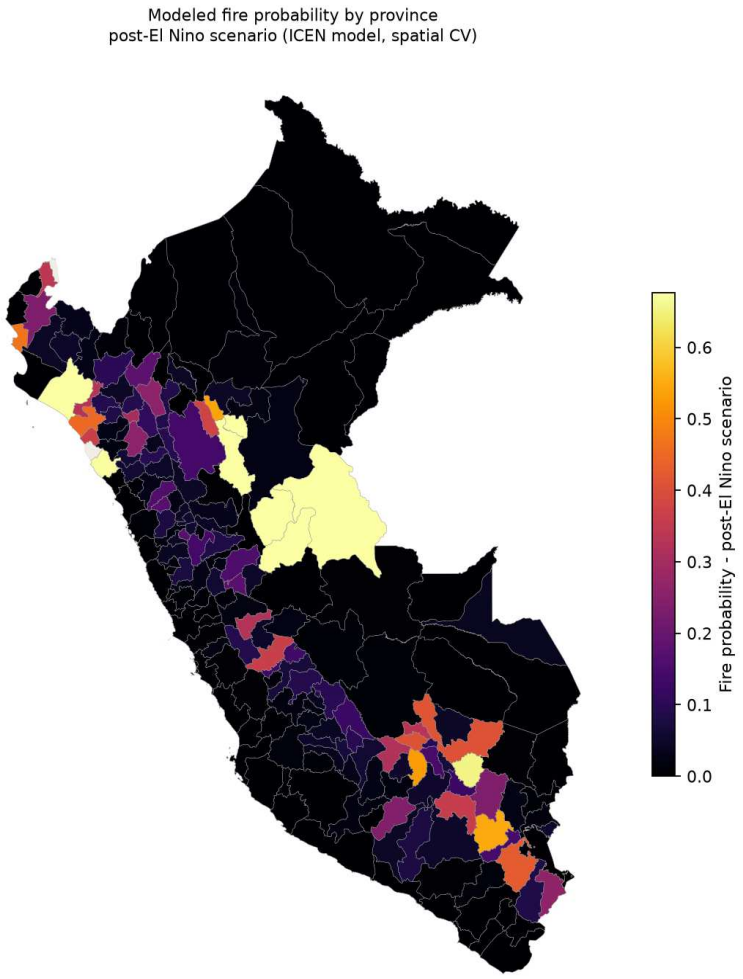


Fig. 22 *Modeled fire probability by province in the post-El Niño scenario*

Future work: cell-level resolution instead of province level (pending export of Earth Engine assets), ENSO x fuel interaction, and incorporation of VIIRS detections for high-Andean grassland fire.

5.8 Robustness and Sensitivity Analysis

This section summarizes four robustness checks performed on the tables of the preceding sections, motivated by the fact that a study with short series (n=24 years) and assumed engineering parameters needs to quantify how much of its conclusions depend on specific methodological choices.

For the correction for multiple comparisons, of the 20 fire-ENSO correlations explored in Section 5.2.1 (4 series x 5 predictors), 2 are significant uncorrected ($p < 0.05$) and none survive Benjamini-Hochberg correction (FDR, $q = 0.05$). The 95% bootstrap confidence interval (10,000 resamples) of the lagged national correlation is [0.09, 0.80], and for the Andes it is [-0.01, 0.76]: compatible with a real effect but with substantial uncertainty given n=24. This exploratory table should be read as hypothesis-generating rather than confirmatory proof; confirmation rests instead on the multiproduct replication (Section 5.2.2) and on the predictive model described next.

The spatial stability of the predictive model was tested by repeating the spatial cross-validation by department with 30 distinct random partitions, shuffling which departments fall into each of the 6 folds; the AUC improvement from ENSO is consistent, with a mean of +0.061 (SD 0.007; 95% percentile CI [+0.049, +0.074]) and never null across the 30 partitions. Temporal validation, the strictest test, uses leave-one-year-out cross-validation (24 folds, each holding out one full ENSO year never seen in training): here the AUC improvement from ENSO drops to +0.014 but remains positive. The gap relative to the +0.061 from spatial CV is expected, since spatial CV shares the year, and therefore the ENSO value, between training and test; both figures are reported so the reader can distinguish how well the model distinguishes departments in a known year from how well it would forecast a never-seen year, which is the operationally relevant use for early warning. Finally, recalculating the WSIS under four alternative weighting schemes, from equal weights to extreme emphasis on a single component, leaves the ranking of priority districts very stable, with a Spearman correlation between 0.76 and 1.00 relative to the baseline scheme and a top-15 critical-district overlap between 77% and 100% depending on the scheme, so the territorial prioritization in Section 5.4 does not depend critically on the choice of weights.

6. Discussion

6.1 An ENSO-Forced Fire Regime with a Lag

Unlike the common 'El Niño = more fires' framing, in Peru the El Niño year itself tends to burn less, and it is the following year and the cumulative conditions that explain the extreme seasons. This reading does not rest on the isolated bivariate correlation, which is exploratory and does not survive correction for multiple comparisons (Section 5.8), but on the convergence of three independent lines of evidence: replication of a single, pre-specified hypothesis (prior-year ONI) across three satellite products (Section 5.2.2); a model with fifteen topography, fuel, climate, and fire-memory covariates in which the two ENSO terms are the most important predictors; and, above all, an out-of-sample predictive improvement that remains positive under the strictest test available, leave-one-year-out temporal validation, which holds out full ENSO years never seen in training, albeit of more modest magnitude (AUC +0.01 to +0.06 depending on the validation scheme; Section 5.8) than suggested by spatial CV alone. The disaster risk management planning window is therefore not the summer of an ongoing El Niño but the following dry season: an ENFEN El Niño forecast should trigger preparation for the fire season 12-18 months later. For fire, ICEN and ONI provide equivalent predictive power; ICEN is preferred as ENFEN's operational index and because it also captures the coast-specific signal (a fine-fuel pulse in the desert and coastal lomas).

6.2 The Constraint Is Not Volume, It Is Delivery and Coverage

The ANA inventory disproves the initial hypothesis of water scarcity: there are ~5,816 hm3 of usable storage across 709 reservoirs (more storage in the Andes than on the coast) and 13,522 operable lakes (>=2 ha) blanketing the cordillera; 94% of reservoirs have fire within 20 km. Aerial-suppression demand is small relative to that supply. The disaster risk management problem is reformulated into three points: (i) 22% of recurrent fire load has no adequate source within a 15 km operational radius, with a critical gap in the northern highlands and the upper Amazon fringe (Piura, Cajamarca, Amazonas, San Martín, Huánuco); (ii) the delivery rate is limited to ~6-7 cycles/h and ~12,000

L/h per helicopter, so the management variable is the number of aircraft and their pre-positioning, not volume; and (iii) there is no regulated contingent allocation of reservoir volume for fire response. Section 5.5 proposes loading points to close gap (i).

6.3 Double Pressure in Post-El Niño Dry Seasons

The critical window combines the dry season that follows an El Niño, when national burned area nearly doubles (factor 1.93; Section 5.6), with the low-water period of reservoirs. The overlap is greatest in the northern highlands and the upper Amazon fringe (Cajamarca, Amazonas, San Martín) and in Madre de Dios, where a post-El Niño amplification of x3 to x7 combines with a low WSIS. The ENFEN El Niño forecast provides 12-18 months of lead time to pre-position aircraft and to enable the loading points from Section 5.5 in these departments.

6.4 Limitations

Eight limitations bound the interpretation of these results. First, the 24-year series has limited statistical power; effect sizes are reported throughout, and we plan to extend the series with GFED (1997-) and VIIRS detections (2012-) and to work at monthly resolution. Second, MODIS MCD64A1 underestimates small fires, high-Andean grassland fires, and understory fires, which is why it is complemented with active-fire detections and FireCCI51 validation. Third, Peru has no dedicated air-tanker fleet, so the logistics component is a scenario and capacity analysis centered on bucket-equipped helicopters and international support. Fourth, there is volume uncertainty for natural water bodies without bathymetry, and contingent allocation depends on water rights and dam safety, both treated parametrically here.

Fifth, the macroregional partition by elevation and longitude thresholds is a first approximation that will be refined with ecoregions and watersheds. Sixth, the accessibility model uses Euclidean distance, and a terrain-cost version accounting for slope and canyons would reduce the estimated coverage; the helicopter parameters (speed, bucket size, fixed cycle time) and WSIS weights are illustrative and will be subjected to sensitivity analysis and validation against real FAP/INDECI operations. Seventh, lake depth is not recorded in the ANA layer, so the 2 ha threshold is a surface-area screen rather than a guarantee of operability, to be refined with satellite bathymetry and the INAIGEM lake inventory. Eighth, the loading points proposed by the MCLP (Section 5.5) are an idealized upper bound, since candidates are the discovered fire cells rather than verified sites with road access, land tenure, or an actual water body; before an operational proposal, candidates must be restricted to feasible sites.

6.5 Transferability

The framework is applicable to Ecuador, Bolivia, and Colombia (tropical Andean countries with marked seasonality and ENSO modulation) and, more broadly, to semi-arid regions with irrigation infrastructure and a seasonal fire regime.

7. Conclusions

Peru's fire regime (2001-2024) is modulated by ENSO with a one-year lag: national burned area correlates negatively with contemporaneous ICEN (rho = -0.36) and positively with the prior year's ONI (rho = +0.50). The latter correlation

does not survive correction for multiple comparisons in isolation, but the same hypothesis is reproduced across three satellite products, and a predictive model with spatial and temporal cross-validation shows a consistent, always-positive AUC improvement from ENSO (+0.01 to +0.06 depending on the validation scheme, Section 5.8); burned area also nearly doubles in the dry seasons that follow an El Niño (factor 1.93). In a province-level model with fifteen covariates, the ENSO terms are the dominant predictors, and the arid coast is the exception, with its maxima occurring in the coastal El Niño years themselves. The ANA inventory (709 reservoirs with ~5,816 hm3 of usable storage, more storage in the Andes than on the coast, and 13,522 operable lakes >= 2 ha) demonstrates that water is not the limiting factor: 94% of reservoirs have fire within <20 km, and the 10% allocable volume (582 hm3) exceeds aerial-suppression demand by several orders of magnitude.

The binding constraint is instead delivery and coverage: 22% of recurrent fire load lacks an adequate source within 15 km, with a critical gap in the northern highlands and the upper Amazon fringe, and the delivery rate is ~6-7 cycles/h and ~12,000 L/h per helicopter, so the management variable is the number of aircraft and their pre-positioning. Twenty well-sited loading points identified by the MCLP would raise national coverage from 78% to 96%, and the territorial priority, based on double pressure from post-El Niño amplification of x3 to x7 combined with a low WSIS, is Cajamarca, Amazonas, San Martín, Madre de Dios, La Libertad, and Tumbes. These results have three implications for SINAGERD, Peru's national disaster risk management system: formally regulating contingent allocation of a percentage of reservoir usable volume for fire response, using ICEN and the ENFEN forecast as a preparedness trigger 12-18 months in advance, and establishing loading points and pre-positioning helicopters in the departments identified here. The framework, open source and built on Google Earth Engine and Python, is reproducible and transferable to the tropical Andes.

References

Barbosa MLF, Delgado RC, de Andrade CF, Teodoro PE, Silva Junior CA, Wanderley HS et al (2021) Recent trends in the fire dynamics in Brazilian Legal Amazon: interaction between the ENSO phenomenon, climate and land use. Environ Dev 39:100648. https://doi.org/10.1016/j.envdev.2021.100648

Defensoría del Pueblo (2024) Informe Defensorial N.° 225: informe de supervisión en el marco de los incendios forestales 2024: impacto, responsabilidad y vulneración de derechos fundamentales. Defensoría del Pueblo, Lima. https://www.defensoria.gob.pe/wp-content/uploads/2024/09/Informe-Defensorial-n.%C2%B0-225-Incendios-forestales.pdf

ENFEN (2012) Definición operacional de los eventos El Niño y La Niña y sus magnitudes en la costa del Perú. Nota Técnica ENFEN, Comisión Multisectorial ENFEN, Lima

Funk C, Peterson P, Landsfeld M, Pedreros D, Verdin J, Shukla S, Husak G, Rowland J, Harrison L, Hoell A, Michaelsen J (2015) The climate hazards infrared precipitation with stations (CHIRPS): a new environmental record for monitoring extremes. Sci Data 2:150066. https://doi.org/10.1038/sdata.2015.66

Giglio L, Boschetti L, Roy DP, Humber ML, Justice CO (2018) The Collection 6 MODIS burned area mapping algorithm and product. Remote Sens Environ 217:72-85. https://doi.org/10.1016/j.rse.2018.08.005

Gorelick N, Hancher M, Dixon M, Ilyushchenko S, Thau D, Moore R (2017) Google Earth Engine: planetary-scale geospatial analysis for everyone. Remote Sens Environ 202:18-27. https://doi.org/10.1016/j.rse.2017.06.031

Hansen R (2012) Estimating the amount of water required to extinguish wildfires under different conditions and in various fuel types. Int J Wildland Fire 21(5):525-536. https://doi.org/10.1071/WF10131

Lehner B, Liermann CR, Revenga C, Vörösmarty C, Fekete B, Crouzet P, Döll P, Endejan M, Frenken K, Magome J, Nilsson C, Robertson JC, Rödel R, Sindorf N, Wisser D (2011) High-resolution mapping of the world's reservoirs and dams for sustainable river-flow management. Front Ecol Environ 9(9):494-502. https://doi.org/10.1890/100125

Pekel JF, Cottam A, Gorelick N, Belward AS (2016) High-resolution mapping of global surface water and its long-term changes. Nature 540:418-422. https://doi.org/10.1038/nature20584

Plucinski MP (2019) Contain and control: wildfire suppression effectiveness at incidents and across landscapes. Curr For Rep 5:20-40. https://doi.org/10.1007/s40725-019-00085-4

SERFOR (Servicio Nacional Forestal y de Fauna Silvestre) (2024) Sistema Nacional de Información Forestal y de Fauna Silvestre (SNIFFS): módulo de monitoreo de incendios forestales. https://sniffs.serfor.gob.pe/monitoreo/. Accessed 15 Sep 2026

Takahashi K, Montecinos A, Goubanova K, Dewitte B (2011) ENSO regimes: reinterpreting the canonical and Modoki El Niño. Geophys Res Lett 38:L10704. https://doi.org/10.1029/2011GL047364

Zeferino JA (2020) Optimizing the location of aerial resources to combat wildfires: a case study of Portugal. Nat Hazards 100(3):1195-1213. https://doi.org/10.1007/s11069-020-03856-6

Statements and Declarations

Funding

The authors declare that no funds, grants, or other support were received during the preparation of this manuscript.

Competing Interests

The authors declare no competing interests.

Author Contributions

Conceptualization: J. Cruz Machacuay, J.C. Breña Aliaga, C.S. Berrios Romero. Methodology: J. Cruz Machacuay, J.C. Breña Aliaga, C.S. Berrios Romero. Software, data curation, formal analysis and visualization: J. Cruz Machacuay. Validation: J.C. Breña Aliaga, C.S. Berrios Romero. Writing – original draft: J. Cruz Machacuay. Writing – review & editing: all authors. All authors read and approved the final manuscript.

Ethics Approval

Not applicable. This study analyses open geospatial, climatic, and hydrological data (satellite remote sensing, geoservices of Peru's National Water Authority, and official oceanographic indices) and involves no human participants or animal subjects.

Consent to Participate

Not applicable.

Consent to Publish

Not applicable.

Use of Artificial Intelligence

Generative AI tools were used for translation support, grammatical correction and language and style improvement during manuscript preparation. They were not used to generate, analyse or interpret data, to design the methodology, or to draft original scientific content or conclusions; all data processing, index computation and interpretation are the authors' own work, and the authors take full responsibility for the final text.

Data Availability

All inputs are openly accessible. The code (Google Earth Engine and Python, plus a Node.js manuscript generator), the reconstructed ENSO indices, the derived tables (including the robustness analyses of Section 5.8), and the figures are deposited on Zenodo with a versioned DOI (code under the MIT license, derived tables under CC-BY-4.0; concept DOI to be assigned upon deposit). Third-party data are not redistributed in full and retain their own licenses and attribution requirements (detailed in the Zenodo deposit's data dictionary): MODIS and VIIRS (NASA LP DAAC), FireCCI51 (ESA CCI), JRC Global Surface Water (European Commission), CHIRPS and TerraClimate (UCSB/USGS, University of Idaho), ESA WorldCover, Copernicus DEM, FAO GAUL, ICEN (IGP/ENFEN), ONI (NOAA CPC), and the WFS geoservices of Peru's National Water Authority.

Code Availability

The Python and Google Earth Engine scripts, and the Node.js script used to generate this manuscript, are included in the same Zenodo deposit as the dataset (Data Availability): https://doi.org/10.5281/zenodo.22776042.